J. Fluid Mech. (2008), *vol.* 603, *pp.* 367–389. © 2008 Cambridge University Press
doi:10.1017/S0022112008001018 Printed in the United Kingdom

Coherent structures in bypass transition induced by a cylinder wake

CHONG PAN, JIN JUN WANG, PAN FENG ZHANG AND LI HAO FENG

Institute of Fluid Mechanics, Beijing University of Aeronautics and Astronautics, Beijing, 100083, China

(Received 19 September 2006 and in revised form 6 February 2008)

Flat-plate boundary layer transition induced by the wake vortex of a two-dimensional circular cylinder is experimentally investigated. Combined visualization and velocity measurements show a different transition route from the Klebanoff mode in free-stream turbulence-induced transition. This transition scenario is mainly characterized as: (i) generation of secondary transverse vortical structures near the flat plate surface in response to the von Kármán vortex street of the cylinder; (ii) formation of hairpin vortices due to the secondary instability of secondary vortical structures; (iii) growth of hairpins which is accelerated by wake-vortex induction; (iv) formation of hairpin packets and the associated streaky structures. Detailed investigation shows that during transition the evolution dynamics and self-sustaining mechanisms of hairpins, hairpin packets and streaks are consistent with those in a turbulent boundary layer. The wake vortex mainly plays the role of generating and destabilizing secondary transverse vortices. After that, the internal mechanisms become dominant and lead to the setting up of a self-sustained turbulent boundary layer.

1. Introduction

Bypass transition exists universally in nature and engineering, and has attracted increasing attention recently. This concept was first proposed by Morkovin (1969), referring to a boundary layer transition where the exponential amplification of Tollmien–Schlichting waves is bypassed. Landahl (1980) and Hultgren & Gustavsson (1981) proposed the concept of transient growth to describe the algebraic growth of disturbance energy in shear flows, and they attributed such transient growth to non-self-adjoint operators of the linearized Navier–Stokes equations that have non-orthogonal eigenvectors. Subsequent studies (e.g. Butler & Farrell 1992; Andersson, Berggren & Henningson 1999; Luchini 2000; Tumin & Reshotko 2001) showed that the associated optimal disturbances which lead to maximum energy amplification are stationary streamwise vortices. On the other hand, Leib, Wundrow & Goldstein (1999), theoretically confirmed that free-stream turbulence can cause the initial linear growth of disturbances inside a laminar boundary layer by solving the linearized unsteady boundary-region equations with free-stream turbulence represented as a superposition of vortical free-stream Fourier modes.

Previous studies have shown that different initial disturbances, e.g. free-stream turbulence (abbreviated as FST), surface roughness and acoustic excitation etc., can all lead to bypass transition. Among them, FST-induced transition has attracted most attention. Numerous experiments (e.g. Hancock & Brandshaw 1983; Mislevy & Wang 1996; Bario & Beral 1998; Fransson, Matsubara & Alfredsson 2005) have verified a strong effect of FST on transition process, where prediction tools have been

established to correlate the intensity of FST with the transition position. Klebanoff modes (Klebanoff, Tidstrom & Sargent 1962; Klebanoff 1971), visualized as the occurrence of elongated streaky structures that are independent of the linear theory of two-dimensional Tollmien–Schlichting waves (Kendall 1985; Alfredsson & Matsubara 1996), have been considered to be the most important coherent structures in the transition process (Matsubara & Alfredsson 2001). The growth and breakdown of these unstable streaky structures leads to turbulent spots (Alfredsson & Matsubara 2000).

If the free stream contains the wake of a bluff body, the underlying wall boundary layer may undergo 'wake-induced transition'. Mayle (1991) introduced this term to indicate the boundary layer transition due to both regular free-stream vortices and periodically passing wake structures. This wake/boundary layer interaction scenario is commonly found in engineering situations, e.g. the interaction between the wake shed from an upstream airfoil/blade and the boundary layer developing over a downstream airfoil/blade in multi-airfoil systems and turbo-machinery.

Early studies on wake/boundary layer interaction mainly focused on the influence of the turbulence intensity of the wake. Savill & Zhou (1983) indicated that the main governing parameter is the level of turbulence intensity in the interaction region. Zhou & Squire (1985) divided the wake/boundary layer interaction into two regimes: the strong interaction case where the wake still contains coherent vortices when interacting with the boundary layer, and the weak interaction case where the interaction occurs far downstream so that the coherent motion in the wake has decayed. Squire (1989) further concluded that the upstream wake increases the overall turbulence level, thus accelerating the transition process. This conclusion may be correct when the wake contains no large-scale vortical structures or coherent motions, i.e. the weak interaction case; however, it should be modified for a strong interaction case, where the role of coherent vortices in the wake should be taken into account.

Doligalski, Smith & Walker (1994) have summarized previous studies on vortex interaction with a wall. When a vortex is convected near a solid surface, it can induce a persistent adverse pressure gradient on the boundary layer, thus stimulating rapidly rising thin plumes of fluid from the surface layer, called 'unsteady separation'. These plumes typically contain concentrated vorticity and often roll up into vortex structures through subsequent strong viscous–inviscid interaction. Provided the vortex is strong enough or close enough to the wall, the unsteady separation and the following formation of new vortical structures is generic for a wide variety of vortex configurations, and will occur over an extensive range of Reynolds number.

If the wake-induced transition process belongs to the strong interaction case, a similar vortex/wall interaction may occur to form new vortical structures in the boundary layer. For this case, the transition process may develop along a path that is different from the Klebanoff mode in FST-induced transition.

Kyriakides *et al.* (1999) experimentally studied a strong wake-induced laminar/turbulent transition over a flat-plate boundary layer. They used a two-dimensional cylinder with diameter D to generate a von Kármán vortex street. This cylinder was horizontally positioned above a flat plate, upstream of its leading edge. The streamwise and wall-normal position of the cylinder was $-1D$ and $2.5D$ from the leading edge, respectively. The appearance of secondary vortical structures in the near-wall region is consistent with previous studies on vortex/wall interaction; however, no streaky structures have been reported by Kyriakides *et al.* Therefore it is difficult to conclude whether the cylinder-wake-induced transition differs from the FST-induced one in transition mechanisms from that study.

Ovchinnikov, Piomelli & Choudhari (2006) carried out a numerical investigation on the cylinder–plate combination model similar to that studied by Kyriakides *et al.* (1999) at three Reynolds numbers Re_D (based on cylinder diameter D). Detailed information on the transitional flow field, such as the mean velocity profile, Reynolds stress development and turbulent kinetic energy budgets was reported. Their results revealed that streaky structures appear inside the boundary layer, which lead to a transition to turbulence at two higher Reynolds number cases. They claimed that although the cylinder-wake-induced transition is similar to FST-induced bypass transition in both the $u_{rms}(y)$ profile and the development of streamwise velocity spectra, these two transition scenarios are distinctly different in the nature of external perturbation and transition mechanism. This conclusion clarified the boundary between the above two types of bypass transition, which was not clear in early studies. However, several questions still remain unclear:

(*a*) *Existence of secondary vortical structure.* Ovchinnikov *et al.* (2006) did not observe any spanwise vortical structures inside the boundary layer, which is inconsistent with the experiment by Kyriakides *et al.* (1999). It should be noted that the test parameters in these two investigations, i.e. the streamwise and wall-normal position of the cylinder, the shape of the flat-plate leading edge and the cylinder Reynolds number, are sightly different (see table 1 for comparison). Therefore, the physical reality of the secondary vortical structures should be verified, and the effect of these parameters should be discussed.

(*b*) *Mechanism of streak formation.* Ovchinnikov *et al.* (2006) reported that the average spanwise spacing of streaks is about $2.5D$ and has a weak Reynolds number dependence. They suggested that these streaks are formed as a result of injection of external wake momentum into the boundary layer by spanwise-periodic deformation of coherent rollers in the cylinder wake. It is, however, widely accepted that the streak spacing in a turbulent wall layer is $\lambda^+ \approx 100$. Moreover, according to the 'hairpin–streak' model proposed by Smith & Walker (1997) the streak spacing is determined by the population and spacing of hairpin vortex legs closest to the wall, which in turn is the result of the balance between the vorticity intensification due to longitudinal stretching and vorticity annihilation due to viscous effect. Although streaks in transitional boundary layer are different from turbulent streaks, it is reasonable to question how and when the streak formation process switches from an external mechanism to an internal self-sustained mechanism.

In the present work, based on Kyriakides *et al.* (1999) and Ovchinnikov *et al.* (2006), we experimentally investigate a boundary layer transition process induced by the wake of a two-dimensional cylinder. Flow visualization and digital image processing are used to focus on different coherent structures in different transition stages. In the following, § 2 introduces the experiment setup. The description of time-averaged statistics of the transitional flow field follows in § 3. Section 4 presents the existence of the secondary transverse vortices in the initial transition stage, and § 5 discusses the formation of primary hairpins and their evolution. Hairpin packets and streaks, as § 6 presents, are dominant structures in the later transition stage, contributing to the turbulence self-sustaining mechanisms. Finally, the conclusion and discussion are given in § 7.

2. Experimental setup

The present experiment is conducted in a low-speed water channel at a free-stream velocity of $U_\infty = 115\,\mathrm{mm\,s^{-1}}$. The size of the working section is

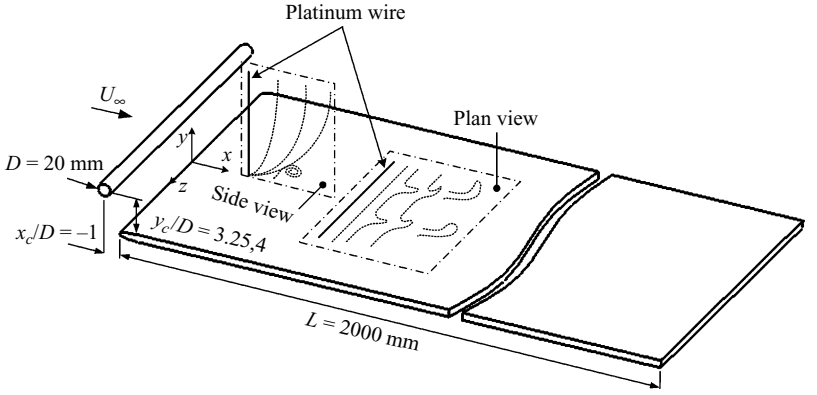

FIGURE 1. Schematic of the experiment arrangement.

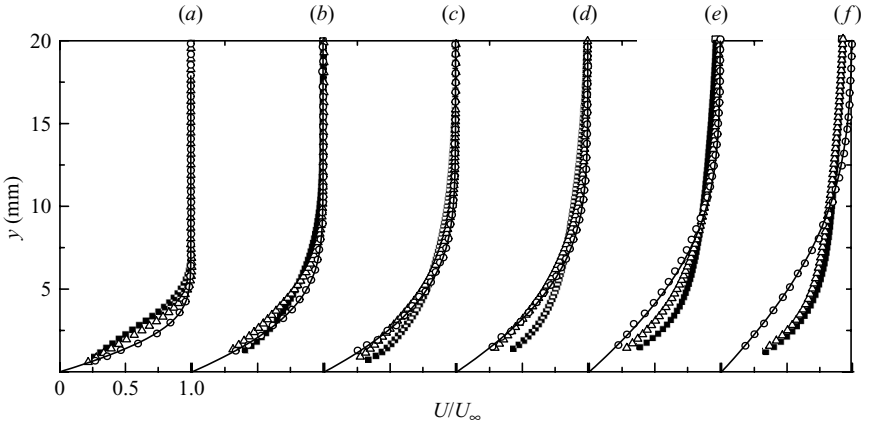

FIGURE 2. Development of mean streamwise velocity profile along the streamwise direction. U is normalized by the free-stream velocity U_∞. ■, $y_c/D = 3.25$; △, $y_c/D = 4$; ○, no cylinder; ——, Blasius solution. (*a*) $x/D = 5$; (*b*) $x/D = 15$; (*c*) $x/D = 25$; (*d*) $x/D = 35$; (*e*) $x/D = 55$; (*f*) $x/D = 75$.

600 mm × 600 mm × 3000 mm (height × width × length) and the free-stream turbulence intensity Tu is about 0.7 % ($Tu = u_{rms}/U_\infty$). Our experimental setup is similar to that of Kyriakides *et al.* (1999) and Ovchinnikov *et al.* (2006), where the wake is generated by a two-dimensional circular cylinder and the boundary layer is developed over the surface of a Plexiglas flat plate with a 4:1 elliptical leading edge. Figure 1 shows the model configuration and the coordinate definitions.

The flat plate has a size of 10 mm × 600 mm × 2000 mm (thick × width × length) and is horizontally positioned 200 mm above the bottom of the water channel. To avoid leading-edge separation, its angle of attack to the free stream is carefully adjusted by a supporting system. Both dye injection and hydrogen bubble visualization reveal that flow around the elliptical leading edge has no separation. Figure 2 shows that the mean velocity profile $U(y)$ of the undisturbed boundary layer agrees well with the Blasius profile up to $x = 1500$ mm downstream, while figure 3 shows that the shape factor H remains almost constant at 2.6. These results indicate that a stable laminar boundary layer develops over the flat plate and no transition occurs throughout the whole region being investigated.

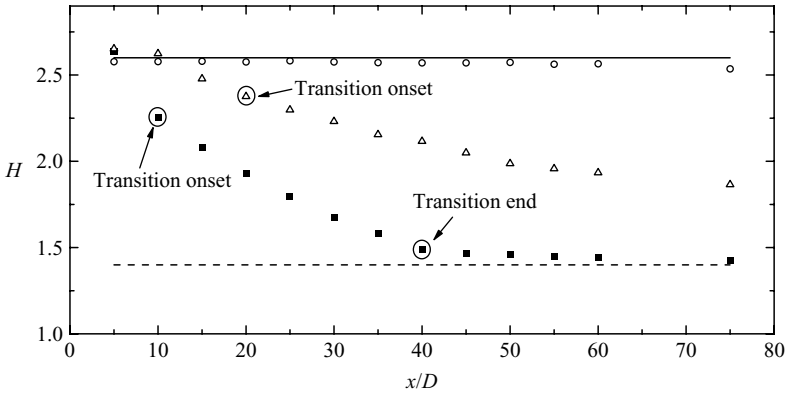

FIGURE 3. Development of shape factor H along the streamwise direction. ■, $y_c/D = 3.25$; △, $y_c/D = 4$; ○, no cylinder; ——, laminar boundary layer; · · · · · ·, turbulent boundary layer.

	Method	LE shape	Re_D	x_c/D	y_c/D	x_{onset}/D	x_{end}/D	$Re_\theta\|_{onset}$	$Re_\theta\|_{end}$
Ovchinnikov *et al.* (2006)	DNS	finite-thickness modelling	385	0	3.5	stable	stable	stable	stable
	LES		1155	0	3.5	30	70	135	200
	DNS		3900	0	3.5	20	40	198	318
Kyriakides *et al.* (1999)	EXP	sharp	3500	−1	2.5	3.3	19	–	–
Present work	EXP	4:1 elliptical	2000	−1	3.25	10	40	124	224
			2000	−1	4	20	> 75	140	> 334

TABLE 1. Comparison of the test parameters and the transition onset/end position with previous studies, where Re_θ is the local Reynolds number based on the momentum thickness θ.

The cylinder is two-dimensional with a diameter of 20 mm and a length of 600 mm. The Reynolds number Re_D is nearly 2000, lying in the subcritical region. Flow over the cylinder undergoes a laminar separation and its wake soon becomes turbulent. The streamwise distance from the cylinder centre to the leading edge is set to be $x_c/D = -1$ with the wall-normal distance varying from $y_c/D = 3.25$ to 4. It should be noted that the present study does not replicate the experiment/simulation by Kyriakides *et al.* (1999) and Ovchinnikov *et al.* (2006), thus the test parameters are slightly different from theirs (see table 1 for comparison). Without the downstream flat plate, the cylinder's vortex shedding frequency ω_{st} is 1.12 Hz, corresponding to the Strouhal number $St = 0.195$ (based on U_∞). With the flat plate in place, ω_{st} increases to 1.22 Hz for the case of $y_c/D = 3.25$ and 1.19 Hz for the case of $y_c/D = 4$. This is consistent with the result from Angrill, Bergamaschi & Cossalter (1982), which revealed that the proximity of a wall to a circular cylinder induces a slight increase of the cylinder vortex shedding frequency.

Hydrogen bubble time-line visualizations are used to investigate coherent structures during the transition process. In the plan view case, a 25 μm diameter platinum wire is set in a holder with a span of 250 mm, and is horizontally positioned inside the boundary layer. In the side view case, the wire is vertically positioned in the symmetric plane, with one end attached to the wall by a 20 μm thick glue tape and the other

end tied onto the tip of a traversing probe to cover the streamwise positions from $x/D = 5$ to 75 with a spacing of 5.

Visualized flow patterns are captured by a digital camera at a frequency of 25 f.p.s. A velocity measurement technique based on the 'time-of-flight' idea has been developed. This idea was first proposed by Lu & Smith (1985), who successfully extracted velocity information from the displacement of two neighbouring hydrogen bubble time-lines in each visualization frame. However, there are some cases in which this technique cannot work well. For example, the neighbouring two time-lines in non-uniform flow with strong shear or turbulence may be twisted or connected, where the time-line edge detection technique fails to discriminate relative displacement. We combine Lu & Smith's (1985) idea with a particle image velocimetry (PIV) measurement technique to implement time-line velocity measurement in a transitional boundary layer. In short, in every visualization frame a group of interrogation windows is distributed parallel to the platinum wire. Each window contains some hydrogen bubbles from a certain time-line. Regarding these hydrogen bubbles as tracer particles, the position of the interrogation window in the next frame can be determined using the spatial cross-correlation maximum searching technique, and its offset between these two frames can be obtained. Since the filming speed is fixed, the Lagrangian average velocity of the interrogation windows can be computed and the instant Eulerian velocity at their origin position can be approximated for a short time interval with a small window size.

This velocity measurement technique is used to deduce quantitative information from side view images in the present visualization. The duration of each visualization set is longer than 210 s, providing more than 5250 frames. The time-line frequency, after a trial-and-error procedure, is set to be 20 Hz. Special care has been taken to ensure that the camera's focal plane is parallel to the bubble sheet. The field of view is about 60 mm in the streamwise direction and 40 mm in the wall-normal direction, corresponding to a spatial resolution of about 0.08 mm pixel^{-1}. Since the non-uniformity of time-line images in the wall-normal direction is much less than that in the streamwise direction, we do not trace the y-offset of interrogation windows for the wall-normal velocity. Owing to the dissipation of older hydrogen bubbles, the reliable velocity measurement area is limited to the first few 'new-born' time-lines. Therefore, we only measure the instant velocity profile along the platinum wire by distributing the interrogation window at 30 pixels behind the wire. Because of the problem of buoyancy and dissipation, few bubbles can enter the near-wall region below $y = 1.5$ mm, so that the closest position where the velocity measurement could be taken is 1.5 mm from the wall.

Analysis of the Basset–Boussinesq–Oseen equation (BBO equation, Hjelmfelt & Mockros 1966), which depicts the motion of discrete particle in viscous fluid, shows that the dynamic response of hydrogen bubbles to fluid velocity fluctuations is correlated with the bubble diameter d_p, i.e. a smaller diameter leading to a better following performance. In the present case, the bubble diameter d_p is about 25 μm, equivalent to that of the platinum wire. With the velocity range of $u < U_\infty = 115$ mm s^{-1}, the upper threshold of the fluctuation frequency which hydrogen bubbles can follow with a maximum relative velocity error of 0.5 % is 150 Hz, and the corresponding time delay of the velocity fluctuation from fluid to bubbles is about 25 μs. Therefore, the dynamic response of hydrogen bubbles is satisfactory.

In order to obtain a high spatial resolution in the wall-normal direction, the window size is set to 13 pixels in the streamwise direction and 2 pixels in the wall-normal direction with a 1 pixel spacing. A direct cross-correlation algorithm, instead of a fast

Fourier transform algorithm, is used to fit this non-standard window size. Gaussian peak fit (Willert & Gharib 1991) is used to enhance the resolution of cross-correlation peak identification to a sub-pixel level; therefore, the uncertainty of the source window offset is estimated to be ± 0.1 pixel, corresponding to a relative error of about 0.2 % in the free-stream velocity. A median filter is used to identify bad points which do not fit the continuity condition. Each velocity datum is compared with the median average of its 3×3 neighbours in the (t, y) plane. If the relative difference exceeds 40 %, this datum is tagged a bad point and replaced by a cubically interpolated value. Comparing to randomly distributed particles in PIV, the present measurement traces parts of the time-lines which have deterministic shape with distinct edge. Therefore, the signal-to-noise ratio is very high, and the cross-correlation maximum searching procedure yields bad points less than 1.5 %. The time-line velocity measurement technique reports a free-stream turbulence intensity of about 0.7 % in the present experiment, which is comparable to the value of 0.73 % measured by a standard two-dimensional PIV system. Both this technique and the PIV system are used to measure a Blasius time-averaged streamwise velocity profile. By comparing the results of these two methods, the whole uncertainty of this time-line velocity measurement technique is estimated to be about 3 %.

3. Mean flow field statistics

Figure 2 presents the development of mean velocity profile $U(y)$ along the streamwise direction for the $y_c/D = 3.25$ and $y_c/D = 4$ case, while figure 3 shows the corresponding evolution of shape factor H. Both show significant influence of the cylinder wake on the boundary layer evolution. For the $y_c/D = 3.25$ case, the $U(y)$ profile initially has a mean velocity deficit at $x/D = 5$ inside the boundary layer, resulting in a slight increase in H beyond 2.6. As shown in § 4, this velocity deficit is mainly related to secondary transverse vortices which are periodically generated near the wall. This velocity deficit quickly diminishes at $x/D = 10$, and the $U(y)$ profile recovers the Blasius level. The transition process begins further downstream, where the $U(y)$ profile becomes blunter, corresponding to a reduction in H.

Traditionally, the transition stage is defined by the spatial distribution of intermittency factor γ. However, the flow characteristic quantity used to calculate γ varies with different flow type and transition scenario, and the laminar–turbulent cutoff threshold is usually objectively selected. For simplicity, the variation of H along the streamwise direction is used as an alternative criterion in the present case. This defines the transition onset where H significantly deviates from the Blasius level ($H = 2.6$) with a local maximum derivative, and the transition end where H begins to converge within 8% difference to the turbulence level ($H = 1.4$). Using this criterion, the transition onset and end for the $y_c/D = 3.25$ case is estimated to be at about $x/D = 10$ and $x/D = 40$, respectively. Owing to the limited streamwise stations measured in the present case, this division about the transition stage is not very precise. However, the following discussion will show that the evolution of both the $u_{rms}(y)$ profile and coherent structures agree with this division, suggesting that such qualitative estimation is acceptable.

With the cylinder height increasing to $y_c/D = 4$, the transition is delayed to further downstream. The initial mean velocity deficit still exists, but it has a smaller magnitude and persists until $x/D = 20$. The transition is estimated to begin at about $x/D = 20$ for this case, and is not complete even at the last measurement ($x/D = 75$).

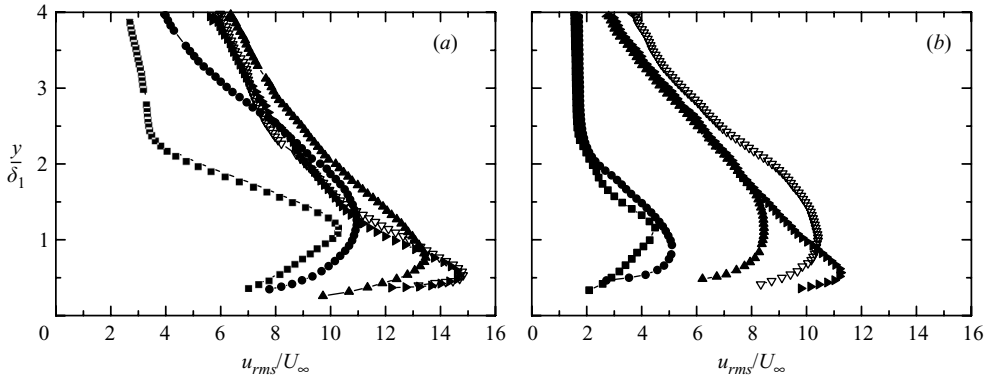

FIGURE 4. Development of $u_{rms}(y)$ profile along the streamwise direction. u_{rms} is normalized by U_∞. (*a*) $y_c/D = 3.25$; (*b*) $y_c/D = 4$. ■, $x/D = 5$; ●, $x/D = 10$; ▲, $x/D = 20$; ▽, $x/D = 40$; ►, $x/D = 50$.

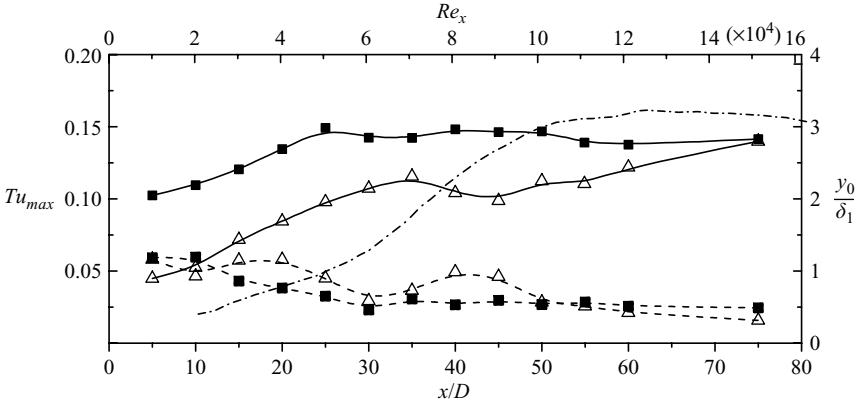

FIGURE 5. Development of Tu_{max} and y_0/δ_1 along the streamwise direction. —■—, Tu_{max} with $y_c/D = 3.25$; —△—, Tu_{max} with $y_c/D = 4$; —·—, Tu_{max} with $y_c/D = 3.5$ $Re_D = 3900$ from Ovchinnikov *et al.* (2006); ···■···, y_0/δ_1 with $y_c/D = 3.25$; ···△···, y_0/δ_1 with $y_c/D = 4$.

Figure 4 shows the downstream evolution of the streamwise velocity fluctuation intensity profile $u_{rms}(y)$, where y is normalized by the local displacement thickness δ_1. For the $y_c/D = 3.25$ case, the pre-transitional $u_{rms}(y)$ profile has an overall upward shift until $x/D = 10$. After the transition begins, the height y_0 of the u_{rms} maximum gradually reduces (see figure 5) as the $u_{rms}(y)$ profile is squashed towards the wall. As the boundary layer develops into turbulence, a self-similarity is achieved, with y_0/δ_1 remaining almost constant and the $u_{rms}(y)$ profiles approximately collapsing onto one curve. For the $y_c/D = 4$ case, the $u_{rms}(y)$ profile develops in a similar way, although the upward shift is delayed to $x/D = 10 - 20$, and no self-similarity is reached even at the last measurement ($x/D = 75$).

Ovchinnikov *et al.* (2006) found that the $u_{rms}(y)$ profile in the pre-transitional boundary layer presents an approximate self-similarity, which was thought to be related to laminar streaks induced by the cylinder wake. However, no self-similarity before the transition onset is observed in the present study. Figure 5 compares the evolution of the maximum turbulence intensity Tu_{max} in the present two cases with that in the case of $Re_D = 3900$, $y_c/D = 3.5$ from Ovchinnikov *et al.* (2006). The

present result of Tu_{max} exhibits an initial rapid growth with a subsequent small decay, followed by another moderate growth. Such secondary growth persists until the end of the measurement for the $y_c/D = 4$ case; while a saturation is reached at about $x/D = 40$ for the $y_c/D = 3.25$ case. The development of Tu_{max} in the present case of $Re_D = 2000$, $y_c/D = 3.25$ is similar to that in the case of $Re_D = 3900$, $y_c/D = 3.5$ from Ovchinnikov *et al.* (2006), where Tu_{max} saturates at a similar level. However, it must be pointed out that comparing to Ovchinnikov *et al.* (2006), the present case ($Re_D = 2000$, $y_c/D = 3.25$) has a relatively higher level of Tu_{max} in the first rapid growth stage. As § 4 will show, this difference is associated with the periodical formation of secondary transverse vortical structures, which introduces periodical acceleration/deceleartion and contributes about 70% of the velocity fluctuation intensity.

4. Secondary transverse vortical structures

Secondary transverse vortical structures are observed in both the $y_c/D = 3.25$ case and the $y_c/D = 4$ case. These vortices are located in the inner boundary layer near the leading edge, and strongly affect the mean statistics of associated flow field.

Figure 6(*a*)–(*f*) shows an example of the generation process of secondary transverse vortices for the $y_c/D = 3.25$ case, while figure 6(*g*) presents the corresponding time variation of the instantaneous $u(y)$ profile at $x/D = 5$ ($x = 100$ mm). During time $t - t + \Delta t$ ($\Delta t = 0.2$ s), the inner part of the $u(y)$ profile gradually inflects towards upstream, with a significant inflection point forming at about $y = 4$ mm. The accumulation of low-speed fluid soon leads to a weak flow separation. This is followed by an eruption of low-speed fluid, after which the inner $u(y)$ profile gradually recovers the undisturbed level. As a result of mean shear stretching and wake vortex induction, this erupted fluid moves towards the wall to roll up into a negative transverse vortex at about $t + 2\Delta t$ (indicated as B in figure 6). Further investigation for the $y_c/D = 3.25$ case shows that the formation of secondary transverse vortices is mainly located at about $x/D = 5 - 10$. While for the $y_c/D = 4$ case secondary transverse vortices are formed in further downstream at about $x/D = 10 - 15$. These new-born vortices are initially two-dimensional, with a straight vortex core-line extending into the spanwise direction (see figure 9).

Figure 7 presents the evolution of the power spectrum of streamwise velocity fluctuation at Tu_{max} location (y_0) for the $y_c/D = 3.25$ case. It shows that the power spectrum at $x/D = 5$ has three frequency peaks, $\omega/\omega_{st} = 0.5$, 1 and 2. The fundamental frequency ($\omega/\omega_{st} = 1$) corresponds to the wake vortex shedding frequency, while the two other frequency peaks, $\omega/\omega_{st} = 0.5$ and 2, are the half and second harmonic, respectively. Further downstream, these three peaks gradually lose their dominance, indicating the breakdown of the initial quasi-periodic velocity signal into an aperiodic one. A similar power spectrum variation is observed for the $y_c/D = 4$ case, although the appearance of three frequency peaks is delayed to about $x/D = 10$.

Ovchinnikov *et al.* (2006) also reported peaks in the power spectrum corresponding to the shedding frequency of the cylinder wake and its second harmonic in the case of $Re_D = 3900$, $y_c/D = 3.5$. They attributed the fundamental frequency to the pressure propagation of the unsteadiness of the cylinder wake shedding. According to the vortex/wall interaction scenario discussed in § 1, a secondary vortical structure may be formed due to the vortex-induced unsteady separation near the wall and the subsequent viscous–inviscid interaction (Doligalski *et al.* 1994). Moreover, Kyriakides *et al.* (1999) found the simultaneous generation of secondary vortices with the passage of wake vortices using an ensemble-average technique. Note that in figure 6(*a–f*) two

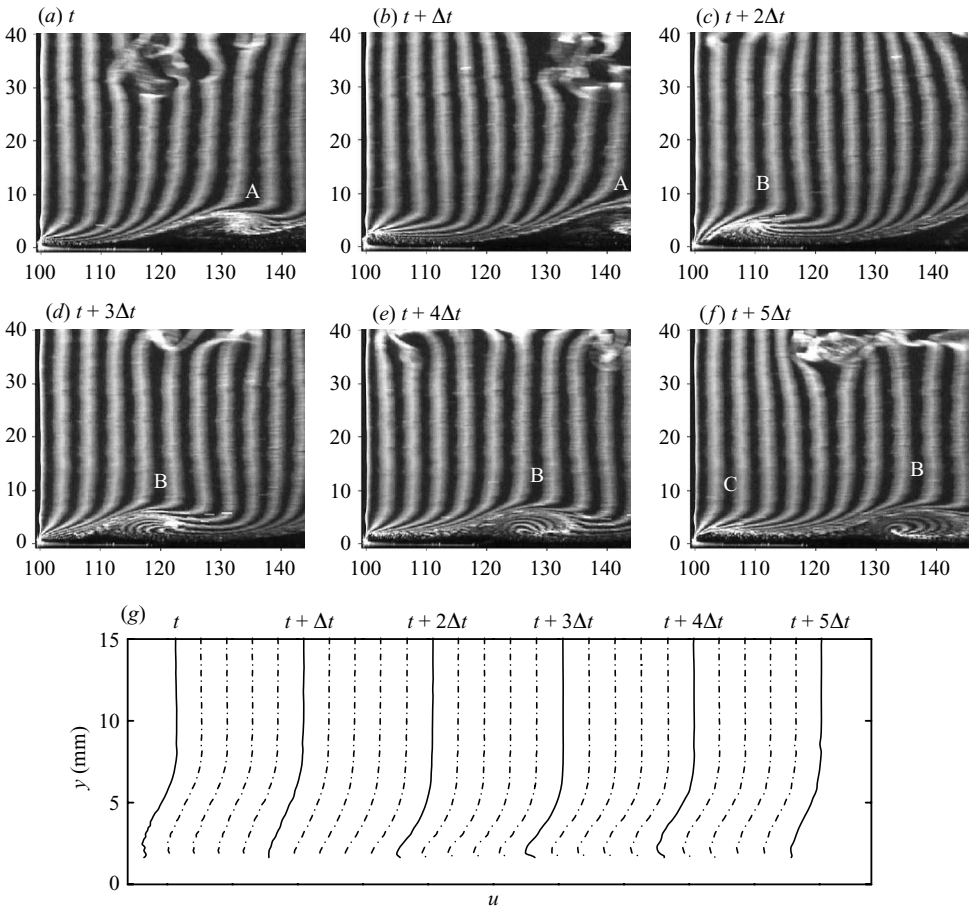

FIGURE 6. Illustration of the generation process of secondary transverse vortices. (a–f) hydrogen bubble side view, $y_c/D = 3.25$, $\Delta t = 0.2$ s, unit: mm; (g) variation of corresponding instantaneous streamwise velocity profile $u(y)$, u is normalized by U_∞.

distinct wake vortices with positive vorticity are observed convecting downstream during the formation of two secondary transverse vortices A and B. This suggests that the fundamental frequency peak corresponds to the periodical generation of secondary transverse vortices, thus indicating a statistical 'one-to-one' relationship between secondary transverse vortices near the wall and wake vortices outside the boundary layer.

The phase-averaged u distribution in the (Φ, y)-plane at $x/D = 5$ is shown in figure 8 for the $y_c/D = 3.25$ case, where Φ is the phase angle. The time variation of u at $y = 6$ mm is used as the phase indicator, based on which more than 280 periods of instantaneous streamwise velocity profiles are traced and phase-averaged. In one phase-averaged period, the whole boundary layer undergoes a successive deceleration/acceleration process, propagating from the inner layer to the outer layer. A low-speed hump appears near the boundary layer edge in the middle of the period. This hump originates from low-speed fluid in the near-wall region due to local separation, and will subsequently evolve into a transverse vortical structure. The low-speed region in the free stream, which indicates the passage of the wake vortex, is well correlated with this hump. Therefore the 'one-to-one' relationship between secondary transverse vortices and wake vortices is further evidenced.

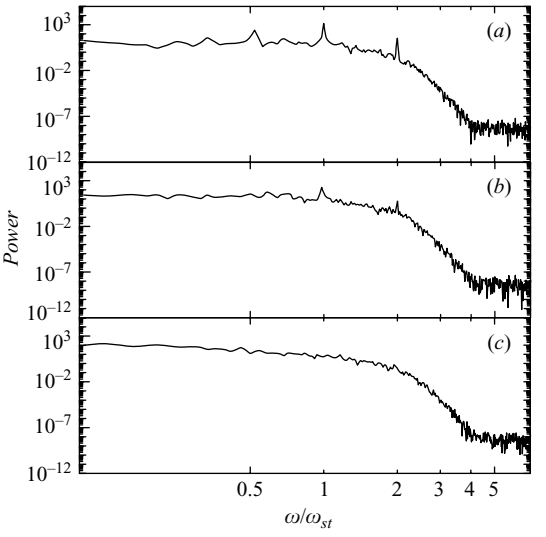

FIGURE 7. Power spectrum of instantaneous streamwise velocity fluctuation at y_0. $y_c/D = 3.25$. (*a*) $x/D = 5$; (*b*) $x/D = 10$; (*c*) $x/D = 25$.

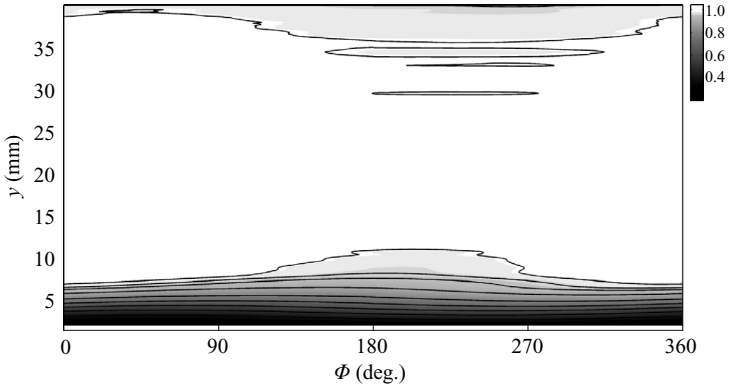

FIGURE 8. Phase-averaged instantaneous streamwise velocity distribution in the (Φ, y)-plane. $y_c/D = 3.25$, $x/D = 5$. u is normalized by U_∞. The time variation of u at $y = 6$ mm is used as the phase indicator.

The effect of secondary transverse vortical structures on the mean flow field statistics near the flat-plate leading edge now seems clear. Being generated as a result of the eruption of low-speed fluid, the secondary transverse vortices contribute to the initial mean velocity deficit inside the boundary layer. The formation of these vortices introduces periodical deceleration/acceleration in the local flow field at the frequency of wake vortex shedding. By subtracting this deceleration/acceleration signal from time trace of u using bandpass filtering, their contribution to the velocity fluctuation intensity is estimated to be 70 % at $x/D = 5$ for the $y_c/D = 3.25$ case and 50 % at $x/D = 10$ for the $y_c/D = 4$ case, thus accounting for a higher level of Tu_{max} in the first rapid growth stage. Moreover, the upward shift of the $u_{rms}(y)$ profile is related to the spatial growth of these vortices and their subsequent lift-up motion. The disappearance of both the mean velocity deficit and the distinct frequency peak downstream suggests a weakening of these structures. Consequently, new mechanisms

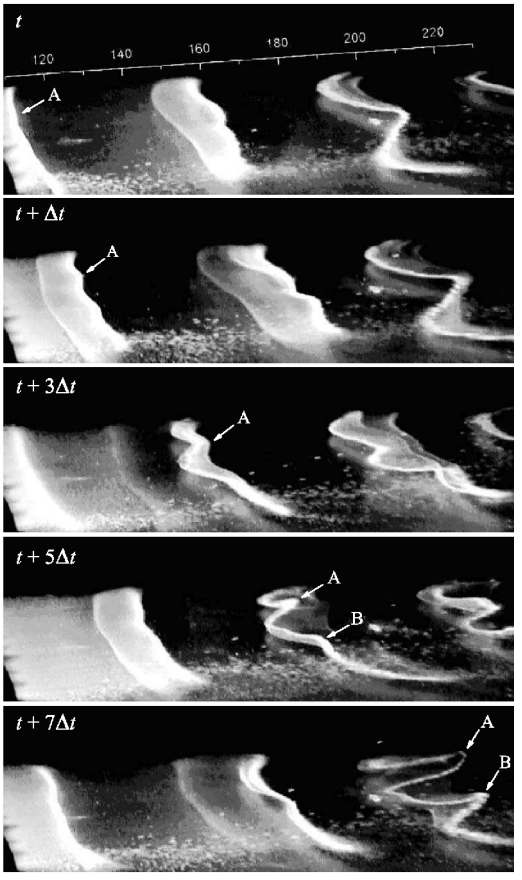

FIGURE 9. Illustration of the generation process of hairpin-like vortices. $y_c/D = 3.25$, plan view, $\Delta t = 0.28$ s, unit: mm. The platinum wire is position at $x/D = 5$, $y = 2$ mm. Free stream flows from the bottom-left to the top-right.

must dominate the transition process to account for the downward shift of the $u_{rms}(y)$ profile.

5. Primary hairpins

Hairpin-like vortices, which are also known as horseshoe vortices, Λ-vortices and ring-like vortices etc., have been accepted as key structures in a turbulent boundary layer which are strongly associated with turbulence self-sustaining mechanisms (e.g. Robinson 1991; Smith & Walker 1997; Zhou *et al.* 1999; Adrian, Meinhart & Tomkins 2000; Adrian 2007). In the present study, hairpins are observed to be directly generated from secondary transverse vortices, hereinafter named primary hairpins. These primary hairpins become dominant coherent structures during transition, where their regeneration and self-organization finally lead to turbulence. In this section, the generation mechanism of primary hairpins is first discussed, followed by a description of their kinematic characteristics.

5.1. *Generation of primary hairpins*

Figure 9 gives an example of the generation process of two hairpins A and B from a secondary transverse vortex for the $y_c/D = 3.25$ case. The bright lines in

the visualization images are the amalgamated hydrogen bubbles due to swirling motion, thus indicating the vortex cores. It shows that the secondary transverse vortex core initially exhibits good two-dimensionality. As it advects downstream, a small non-uniformity appears in the vortex core, which is soon amplified due to vortex instability of multi-inflection points. Some parts of the transverse vortex (e.g. the part indicated by arrow A at $t + 3\Delta t$, where $\Delta t = 0.28$ s) can be sufficiently accelerated, thus significantly protruding downstream. Owing to the background mean shear, the flow acceleration is always coupled with lift-up motion. Therefore, the downstream protruded part lifts up to be further accelerated, while its neighbouring part is still retarded in the near-wall region. The mean shear stress in the boundary layer results in the tilting of the transverse neck which connects the lifted high-speed part and the retarded low-speed part. At $t + 5\Delta t$, a Λ-shaped structure indicated by arrow A is moving away from the original vortex. Further downstream at $t + 7\Delta t$, its legs undergo continuous streamwise stretching, while its head bends back and upward to form a hairpin-like vortex. Another Λ-shaped vortex (indicated by arrow B) is being formed from the same secondary transverse vortex, indicating that several hairpins can move away from one transverse vortex.

Our investigation for the $y_c/D = 3.25$ case shows that the three-dimensional distortion of secondary transverse vortex cores usually occurs after $x/D = 7$, and hairpin-like structures begin to appear after the transition onset ($x/D = 10$). When the cylinder height increases to $y_c/D = 4$, the two-dimensionality of secondary transverse vortices persists over a longer distance, while the formation of hairpin-like structures occurs further downstream at about $x/D = 20$.

No hairpin-like structures have been reported in previous studies on FST or wake-induced boundary layer transition. Hon & Walker (1991) numerically examined the three-dimensional distortion of a spanwise vortex over a plane wall. They found that a line vortex containing a small three-dimensional disturbance would develop into a complex hairpin-like shape with subsidiary hairpin vortices forming outboard. The present formation scenario of hairpins from secondary transverse vortices agrees well with what Hon & Walker (1991) reported, thus suggesting the physical validity of the presence of these primary hairpins.

Because of the difficulty in investigating dynamic behaviour of hairpins in fully developed turbulent boundary layer, previous kernel experiments/simulations studied hairpins artificially generated in laminar environment using wall-bounded hemisphere or continuous/pulse injection (e.g. Acarlar & Smith 1987*a*, *b*; Haidari & Smith 1994; Singer & Joslin 1994; Skote, Haritonidis & Henningson 2002; Svizher & Cohen 2006). These studies showed satisfying similarities between laminar hairpins and turbulent ones in both vortical shapes and developing dynamics. To interpret the artificial generation mechanisms of hairpin structures, numerical/theoretical investigations on the evolution of localized vortical disturbance in viscous shear flow have been carried out by Suponitsky, Cohen & Bar-yoseph (2005) and Shukhman (2006, 2007). Their results revealed that a large-amplitude disturbance, independent of its initial geometrical shape, can eventually evolve into a hairpin vortex. Moreover, Svizher & Cohen (2006) concluded that the generation of hairpins under various base flow conditions is governed by a basic mechanism, the important common elements of which are the shear of the base flow and a sufficiently large initial disturbance. Compared with those 'well-controlled' hairpins generated by surface or velocity modulation, the present primary hairpins exhibit a 'quasi-natural' behaviour. However, their generation mechanism is similar to that concluded by Svizher & Cohen (2006): the initial three-dimensional disturbances on the secondary transverse vortices seem

to be related to the cylinder wake vortices, while the inner dynamical mechanisms, including both the vortex instability and the mean shear stretching, dominate the subsequent formation.

5.2. *Subsequent evolution*

Acarlar & Smith (1987*b*) concluded from their experiment that 'well-controlled' hairpins lift up during their evolution. This is the result of a balance between two opposite effects: the mutual induction between two counter-rotating legs and the head which provides an upstream-outward induction force; and the mean shear of the boundary layer, which results in a downstream-downward rotation. They also reported that the narrowing of the middle portion of counter-rotating legs significantly reduces their vorticity, which in turn reduces the mutual induction effect. Consequently, these parts would be pushed downward to the wall, thus creating a 'kinked neck'. Moreover, once the hairpin heads break away from the boundary layer, the shear effect would cease, leaving the mutual induction to take effect to curl the hairpin head back upstream.

The dynamic similarities between the 'well-controlled' hairpins and those in a fully developed turbulent boundary layer suggest that there is an important universality in the balance of the mutual-induction effect and the shear effect. However, the present experiment reveals that positive wake vortices also contribute to the evolution of hairpins. The induction from wake vortices is named 'wake-vortex induction'. It provides an upward force, whose strength depends on the distance between wake vortices and hairpin heads.

Inside the boundary layer, hairpins experience only a weak induction force from wake vortices; therefore, their evolution dynamics is dominated by the mutual-induction and the shear effect. This gives a similar trend to that found by Acarlar & Smith (1987*b*) and Haidari & Smith (1994). Figure 10 gives an example of the evolution of three successive hairpin structures for the $y_c/D = 3.25$ case, where figures 10(*b*) and 10(*c*) show two instantaneous side view images and figure 10(*a*) presents the corresponding u contour in the (t, y)-plane. Three velocity humps in figure 10(*a*) represent three hairpins with a concentrated transverse vortex tube for the head and streamwise-oriented legs. The first hairpin A is an isolated one. Its head curls upstream and quickly grows in size, while its neck undergoes continuous kinking and shrinking, which presents a snake-like shape at $t + \Delta t$ (see figure 10*b*), resembling the schematic sketch by Acarlar & Smith (1987*b*) in their figure 22(*c*). The second hairpin B also has a curled head and kinked neck at $t + 4\Delta t$. Moreover, its size and growth rate are similar to hairpin A, indicating that these two are both primary hairpins directly generated from secondary transverse vortices. A small hairpin C closely follows hairpin B at a lower position, and forms a uniform momentum zone together with B (see figure 10*a*). Adrian *et al.* (2000) have shown that hairpin packets in the outer layer have small velocity dispersion within the interior of the packet envelope, thus forming 'zones of uniform momentum' (Meinhart & Adrian 1995). Therefore, it may be inferred that hairpin C is generated by the primary hairpin B through a parent-offspring scenario (to be discussed in § 6), which subsequently organizes into a hairpin packet together with B.

Once hairpin heads break away from the boundary layer, the wake-vortex induction would play a dominant role as the shear effect ceases. Figure 11 demonstrates such circumstance by showing typical trajectories of eight hairpin heads for the $y_c/D = 3.25$ and $y_c/D = 4$ case. All these hairpins are primary ones, as confirmed by side view visualization. They appear in early transition stage, where the trajectories of

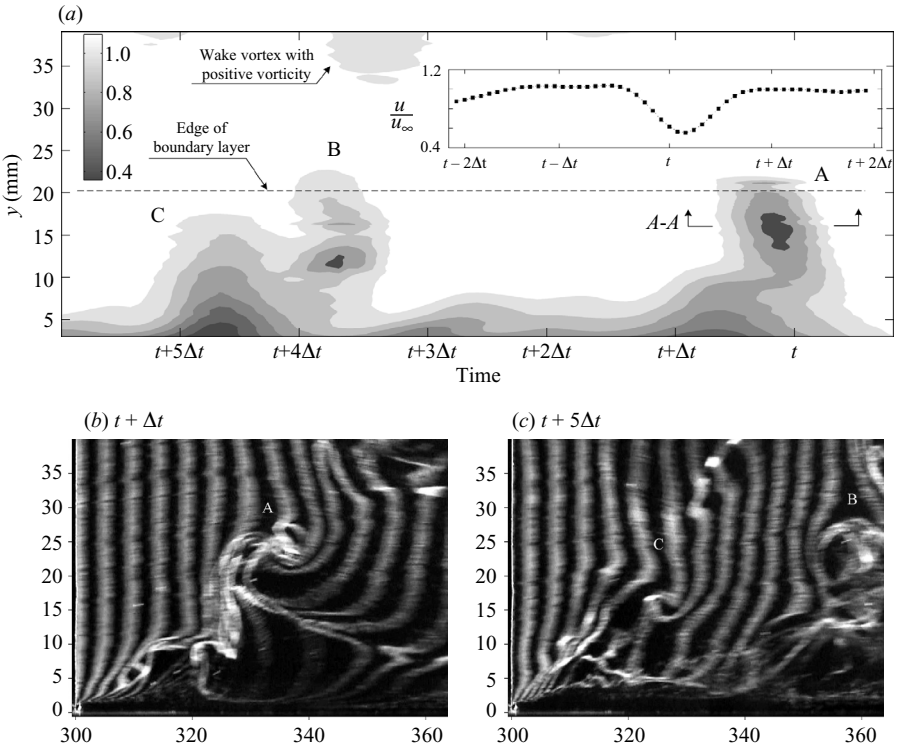

FIGURE 10. Illustration of the evolution of hairpins. $y_c/D = 3.25$, $\Delta t = 0.5$ s. (*a*) contour of instantaneous streamwise velocity u in the (t, y) plane, where u is measured at $x = 300$ mm $(x/D = 15)$ and normalized by U_∞; (*b–c*) the corresponding flow pattern in side view, unit: mm.

their heads are traced by spatial cross-correlation maximum searching technique as discussed in § 2. Due to the uncertainty in their position, these trajectories have some scatter. However, all are linear in the (x, y)-plane, consistent with previous observation by both Haidari & Smith (1994) and Svizher & Cohen (2006). Haidari & Smith (1994) showed that the inclination angle of trajectory of ejection-generated hairpin heads varies from 2.9° to 6.6°, which is strongly correlated with injection parameter and the Reynolds number. Svizher & Cohen (2006) reported an inclination angle of about 5° in a subcritical channel flow. They also found that the increase in injection velocity pushes the trajectory further away from the wall instead of altering the inclination angle. Compared with their results, the present inclination angle (indicated as α in figure 11) is slightly higher. This discrepancy may be attributed to the existence of wake-vortex induction in the present case, which introduces additional lift-up induction to hairpin heads. Moreover, the inclination angle α in figure 11 endures a continuous increase as the height of hairpin heads increases, which is especially significant once the hairpin heads move outside the boundary layer. It is also noted that α decreases as the cylinder height increases from $y_c/D = 3.25$ to 4. Therefor, the strength of wake-vortex induction effect is negatively correlated with the distance between wake vortices and hairpin heads.

To further demonstrate the effect of wake-vortex induction on hairpin heads, ensemble-averaged convection velocity profile of hairpin heads is shown in figure 12. Twenty primary hairpins evolving at $x/D = 20 - 25$ for the $y_c/D = 3.25$ case have

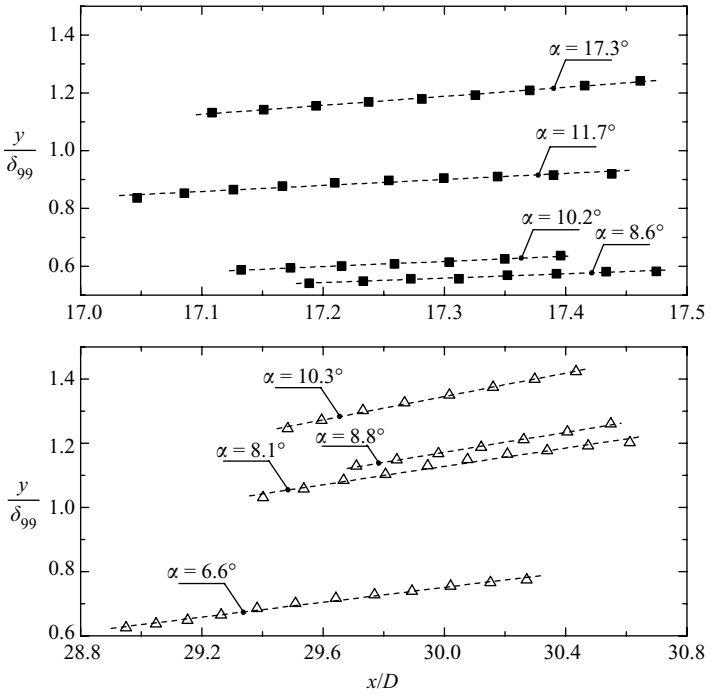

FIGURE 11. Trajectories of primary hairpin heads. ■, $y_c/D = 3.25$; △, $y_c/D = 4$; ·····, linear fit.

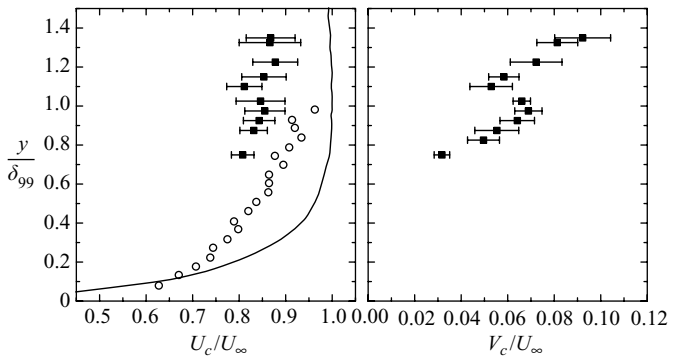

FIGURE 12. Variation of streamwise/wall-normal component of ensemble-averaged convection velocity of primary hairpin heads with wall-normal direction in the streamwise range of $x/D = 20 - 25$. U_c and V_c are both normalized by U_∞. ■, $y_c/D = 3.25$; ○, data from Adrian; ——, $U(y)$ at $x/D = 20$; the error bar shows the statistical variance from mean value.

been traced, and the data from Adrian *et al.* (2000) in a turbulent boundary layer are included for comparison. It should be noted that the boundary layer thickness δ_{99} at $x/D = 20 - 25$ is relatively small and these hairpins are generated directly from secondary transverse vortices; therefore the wall-normal positions y/δ_{99} of these hairpin heads are somewhat greater than those in fully developed turbulence from Adrian *et al.* (2000). Generally speaking, both the streamwise and wall-normal velocity components, U_c and V_c, are positively correlated with the height of hairpin heads, indicating a continuous lift-up motion. The present U_c inside the boundary layer

is much less than that of Adrian *et al.* (2000), which is remarkably close to local mean velocity profile. This discrepancy may be attributed to the fact that the present measurement is carried out in the initial rapid growth stage of transition, where hairpins have not contributed to the mean velocity profile. Inflection points in both U_c and V_c profiles appear near the boundary layer edge, suggesting a loss of the equilibrium between the three induction effects. A rapid increase of V_c outside the boundary layer indicates a ceasing of the mean shear effect and an intensification of the wake-vortex induction, leading to an increase in the inclination angle of hairpin head trajectories as shown in figure 11.

6. Hairpin packets and streaks

Section 5 revealed that the present primary hairpins have a similarity in both the generation mechanism and subsequent evolution process to artificially generated hairpins or those in a fully developed turbulent boundary layer. Therefore, it is reasonable to expect that the regeneration scenario of primary hairpins should be also similar to that documented in Haidari & Smith (1994), Zhou *et al.* (1999) and Adrian *et al.* (2000).

Flow visualization shows that primary hairpins can generate new hairpins through the parent–offspring scenario (Schoppa & Hussain 2002). This regeneration process can be characterized as follows (see figure 13). As primary hairpins convect downstream, their counter-rotating legs are stretched in the streamwise direction and pushed downward to the wall due to shear mechanism. Vortex/wall interaction scenario, which also contributes to the formation of secondary transverse vortices in § 4, results in the gradual accumulation of low-speed fluid beneath or between these legs. Unsteady separation soon occurs, leading to an abrupt eruption of accumulated low-speed fluid. This erupted fluid presents a trajectory inflecting towards the wall through viscous-inviscid interaction mechanism (figure 13(*e*)), and finally roll up into new hairpins (figure 13*d*).

Zhou *et al.* (1999) have demonstrated that a sufficiently strong hairpin is capable of generating a packet of hairpins. At the end of the rapid growth stage of the present transition process, a number of hairpins are found to cluster into packet pattern, where the first one is always primary hairpin and the rest are those generated by the first hairpin. Figure 14(*a–b*) show a typical flow pattern of hairpin packets at $x/D = 20-27.5$ for the $y_c/D = 3.25$ case. Two hairpin packets, indicated as II and III, are visualized during $t - t + \Delta t$ ($\Delta t = 0.4$ s). Each of them contains three individual hairpins and has a characteristic growth angle (defined as the envelope angle of the packet, Adrian *et al.* 2000) of about 11.3° and 16.2°, respectively. The present hairpin packets have a similar shape with that of Adrian *et al.* (2000) as shown in figure 14(*c*), which illustrates a nested hierarchy of hairpin packets in turbulent boundary layer.

Long lasting low-speed streaks begin to appear in the inner layer after $x/D = 25$ for the $y_c/D = 3.25$ case, where the transition completes the first rapid growth stage. Figure 15 shows a streamwise elongated low-speed streak behind a hairpin packet within the counter-rotating pair of legs. The length scale of this streak is equivalent to that of the hairpin packet. Adrian (2007) argued that the regeneration mechanism of hairpin vortices offers an explanation to the contradiction that individual hairpins have length scale almost one order smaller than that of streaks. Our visualization shows that low-speed streaks always follow hairpin packets, further supporting the idea that continuous lift-up inducement by legs of a packet of hairpins is a sufficient condition for the generation of streaks.

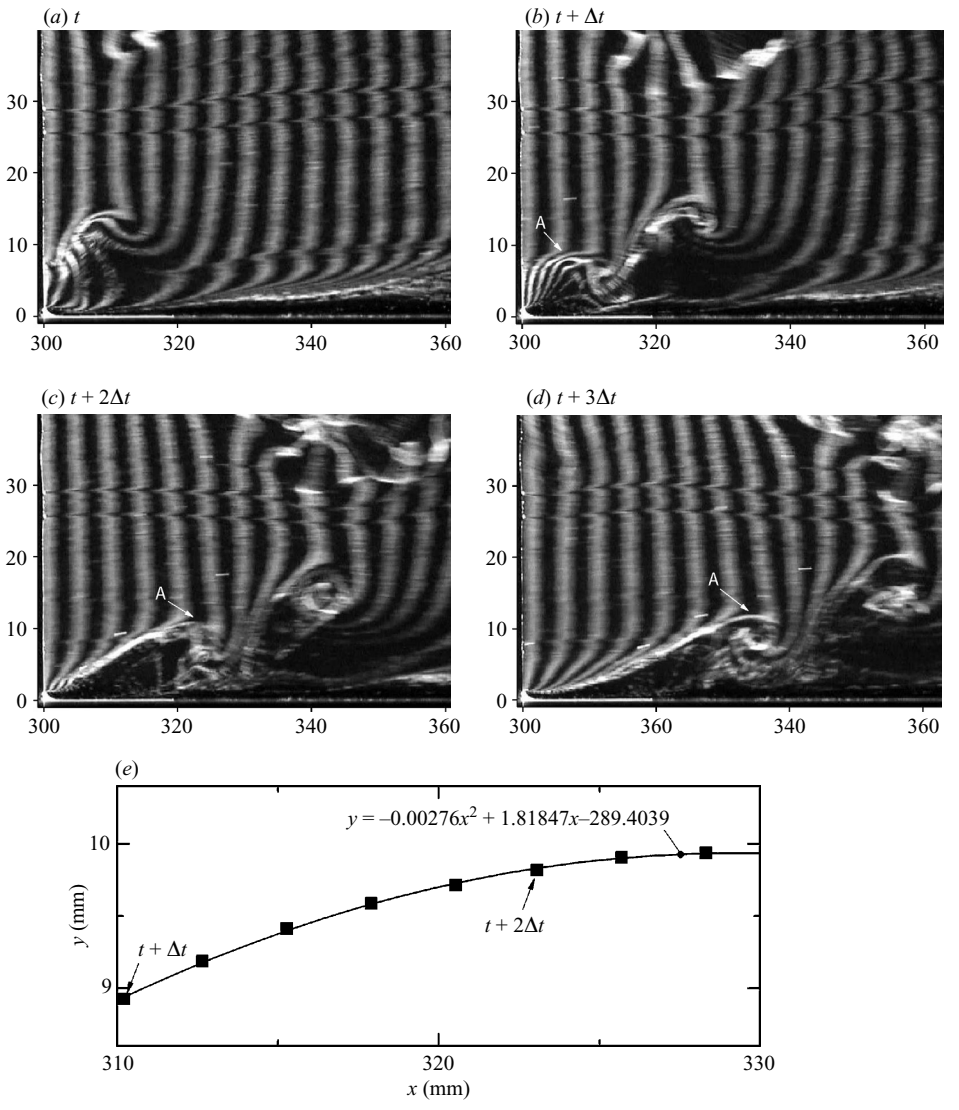

FIGURE 13. Eruption process of low-speed fluid due to the passage of primary hairpin legs. $y_c/D = 3.25$, $\Delta t = 0.2$ s. (*a–d*) side view visualization image series, unit: mm; (*e*) trajectory of the erupted low-speed fluid indicated by A.

In the later stage of the transition process, the varicose instability of low-speed streaks which leads to the formation of high-order hairpins (Asai *et al.* 2002) are commonly visualized. The bursting process of streaks feeds concentrated vorticity into the outer layer (Smith & Walker 1997), thus providing a feedback mechanism to strengthen the regeneration process of hairpin packets. In this way, hairpin packets prevail in outer part of the boundary layer, while streaky structures occupy the inner part, leading to the setting up of a self-sustained turbulent boundary layer.

7. Summary and discussion

The present experiment reveals a wake–vortex-induced boundary layer transition scenario which is different from the Klebanoff mode in FST-induced transition. This

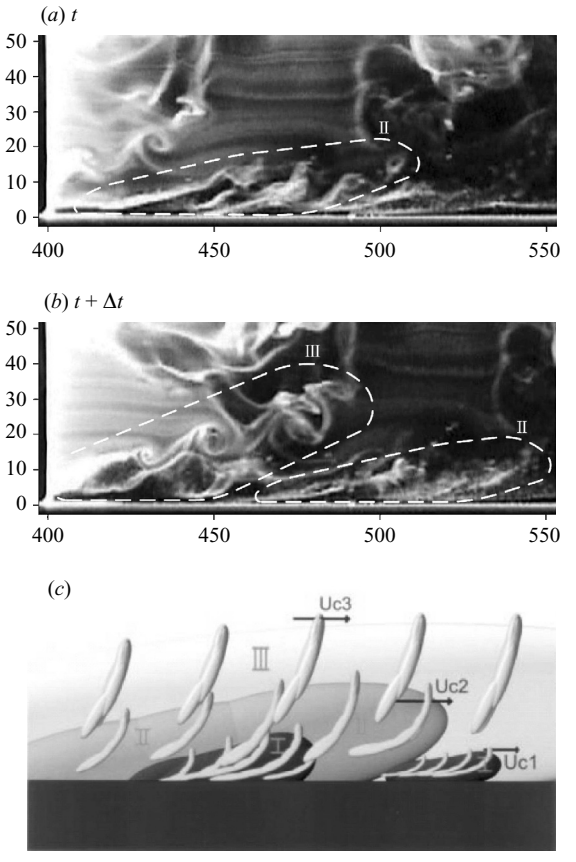

FIGURE 14. Comparison of the flow pattern of hairpin packets in the present transitional boundary layer with those in turbulent boundary layer. (*a–b*) Side view images of hairpin packets, $y_c/D = 3.25$, $\Delta t = 0.4$ s, unit: mm; (*c*) idealized model of nested hierarchy of hairpin packets in turbulent boundary layer from Adrian *et al.* (2000).

transition process is mainly characterized as follows: (i) generation of secondary transverse vortical structures near the flat plate surface in response to the von Kármán vortex street; (ii) formation of hairpins due to the secondary instability of secondary vortical structures; (iii) growth of hairpins which is accelerated by wake-vortex induction; (iv) formation of hairpin packets and the associated streaky structures which is consistent with those in a turbulent boundary layer in both the regeneration kinematics and self-sustaining mechanisms.

The secondary transverse vortices are found to be periodically formed immediately downstream of the leading edge. These vortices have 'one-to-one' correspondence to cylinder wake vortices, and their generation process is similar to the vortex/wall interaction scenario (Doligalski *et al.* 1994). These vortices introduce both a near-wall mean velocity deficit in the $U(y)$ profile as well as local enhancement of the maximum turbulence intensity Tu_{max}. Moreover, the overall lift-up in the $u_{rms}(y)$ profile is a result of the outward motion of these vortices.

Primary hairpins are observed moving directly away from the secondary transverse vortices. It seems that their generation process belongs to the generic mechanism proposed by Svizher & Cohen (2006), i.e. the sufficient initial disturbance induced

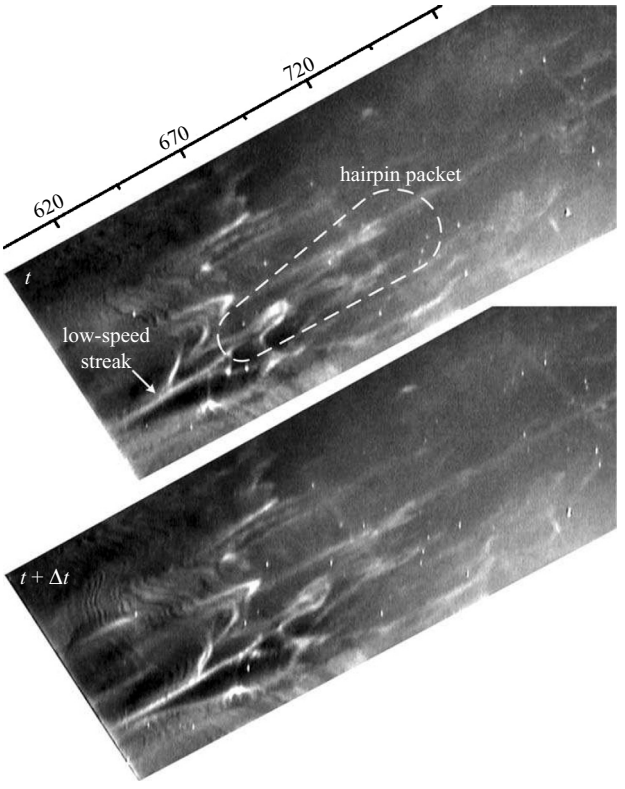

FIGURE 15. Plan view visualization of streaks under leg pairs of a hairpin packet. $y_c/D = 3.25$, $\Delta t = 0.2$ s, unit: mm. The platinum wire is positioned transversely at $x/D = 30$ and $y_w = 2$ mm. Free stream flows from the bottom-left to the top-right.

by wake vortices, followed by the instability developing on the secondary transverse vortices and the subsequent mean shear stretching. After generation, hairpin heads are affected by three induction forces: the mutual induction, the mean shear effect and the wake-vortex induction. The last force accelerates the lift-up motion of hairpin heads which become more significant outside the boundary layer. On the other hand, the hairpin leg pairs are continually stretched in the streamwise direction and pushed toward the wall. When these legs move close enough to the wall, a strong vortex/wall interaction takes place to induce abrupt eruption of low-speed fluid. This leads to a roll-up of new hairpins due to the viscous–inviscid interaction mechanism. The wallward shift of the $u_{rms}(y)$ profile may be associated with the movement of hairpin legs toward the wall. However, further evidence is needed to support this conjecture.

In the later stage of the transition process, hairpins are found to have similar characteristics to artificially generated hairpins as well to those in turbulent boundary layer. They tend to group together to form hairpin packets, which have sufficient induction force to lift up underlying low-speed fluid. This generates low-speed streaks with large length scale, which in turn intensify the regeneration process of hairpin structures.

Ovchinnikov *et al.* (2006) did not report transverse vortical structures in their simulation for any investigated Reynolds numbers; instead, they attributed the generation of streaky structures to the direct impingement of external wake momentum into the boundary layer. We expect that the occurrence of secondary

transverse vortices may have altered the transition scenario quite significantly. Because of the different test parameters, e.g. Re_D, y_c/D, x_c/D and the shape of the leading edge, direct comparison between the present result and that from Ovchinnikov *et al.* (2006) cannot be made. However, owing to the vortex/wall interaction scenario (Doligalski *et al.* 1994), the formation of new vortical structures in the near-wall region would take place over an extensive range of Reynolds number, as long as the vortex is strong enough or close enough to the wall. Also, the difference in x_c/D does not change the characteristics of the strong interaction between the wake vortex and the boundary layer. With y_c/D increasing to 4, the generation of secondary transverse vortices occurs in further downstream, which leads to a delay in the transition process, including the appearance of primary hairpins, hairpins packets and streaks. Therefore, the difference in Re_D, x_c/D and y_c/D may not account for the lack of secondary transverse vortices in Ovchinnikov *et al.* (2006).

We notice that Ovchinnikov *et al.* (2006) used an artificially imposed boundary condition around the leading edge, which smoothly changes from a free-slip condition to a no-slip one over a length of $x/D \approx 8$. This might anchor the stagnation point of the leading edge and alter the receptivity process near the leading-edge. Therefore, it can be inferred that the difference in the leading-edge flow field contributes in the discrepancy in the existence of secondary structures. However, further investigation on the flow field in the leading-edge region is needed to support this conjecture, and the effect of the leading-edge shape should be also examined. Moreover, Kendall (1990) showed that the bluntness of the leading-edge influences the TS-wave generation. Goldstein, Leib & Cowley (1992) theoretically revealed that the leading-edge receptivity to free-stream vorticity gives rise to small-amplitude, nonlinear spanwise motion in the downstream boundary layer. Westin *et al.* (1998) regarded the receptivity to vortical free-stream disturbances as highly dependent on the flow close to the leading edge. Nagarajan, Lele & Ferziger (2007) showed that the onset and completion of the bypass transition induced by FST moves upstream with increasing leading-edge bluntness. Compared to these works, the present study reveals that with the existence of secondary transverse vortices the transition may develop in a way different from the Klebanoff mode, thus further supporting the point of view that the leading-edge receptivity can significantly affect the downstream flow.

This work has been supported by the National Natural Science Foundation of China (no. 10425207 and no. 10602007). The authors are grateful to Professor Kwing-so Choi for his critical suggestion for the revision of the manuscript and Professor Yury S. Kachanov and Dr Vladimir Borodulin for their discussion on PIV-based visualization image processing technique.

REFERENCES

Acarlar, M. S. & Smith, C. R. 1987*a* A study of hairpin vortices in a laminar boundary layer. Part 1. hairpin vortices generated by a hemisphere protuberance. *J. Fluid Mech.* **175**, 1–41.

Acarlar, M. S. & Smith, C. R. 1987*b* A study of hairpin vortices in a laminar boundary layer. Part 2. hairpin vortices generated by fluid injection. *J. Fluid Mech.* **175**, 43–83.

Adrian, R. J. 2007 Hairpin vortex organization in wall turbulence. *Phys. Fluids* **19**, 041301.

Adrian, R. J., Meinhart, C. D. & Tomkins, C. D. 2000 Vortex organization in the outer region of the turbulent boundary layer. *J. Fluid Mech.* **422**, 1–54.

Alfredsson, P. H. & Matsubara, M. 1996 Streaky structures in transition. In *Proc. Conf. on Transitional Boundary Layers in Aeronautics* (ed. R. A. W. M. Henkes & J. L. van Ingen). Royal Netherlands Academy of Arts and Sciences, Elsevier.

Alfredsson, P. H. & Matsubara, M. 2000 Free-stream turbulence, streaky structures and transition in boundary layer flow. *AIAA Paper* 2000-2534.

Andersson, P., Berggren, M. & Henningson, D. S. 1999 Optimal disturbances and bypass transition in boundary layers. *Phys. Fluids* **11**, 134–150.

Angrill, F., Bergamaschi, S. & Cossalter, V. 1982 Investigation of wall induced modifications to vortex shedding from a circular cylinder. *Trans. ASME: J. Fluids Engng* **104**, 518–522.

Asai, M., Minagawa, M. & Nishioka, M. 2002 The instability and breakdown of a near-wall low-speed streak. *J. Fluid Mech.* **455**, 289–314.

Bario, F. & Beral, C. 1998 Boundary layer measurements on the pressure and suction sides of a turbine inlet guide vane. *Expl Therm. Fluid. Sci.* **17**, 1–9.

Butler, K. M. & Farrell, B. F. 1992 Three-dimensional optimal perturbations in viscous shear flow. *Phys. Fluids* A **4**, 1637–1650.

Doligalski, T. L., Smith, C. R. & Walker, J. D. A. 1994 Vortex interactions with walls. *Annu. Rev. Fluid Mech.* **26**, 573–616.

Fransson, J. H. M., Matsubara, M. & Alfredsson, P. H. 2005 Transition induced by free-stream turbulence. *J. Fluid Mech.* **527**, 1–25.

Goldstein, M. E., Leib, S. J. & Cowley, S. J. 1992 Distortion of a flat-plate boundary layer by free-stream vorticity normal to the plate. *J. Fluid Mech.* **237**, 231–260.

Haidari, A. H. & Smith, C. R. 1994 The generation and regeneration of single hairpin vortices. *J. Fluid Mech.* **277**, 135–162.

Hancock, P. E. & Bradshaw, P. 1983 The effect of free-stream turbulence on turbulent boundary layers. *Trans. ASME: J. Fluids Engng* **105**, 284–289.

Hjelmfelt, A. T. & Mockros, L. F. 1966 Motion of discrete particles in a turbulent fluid. *Appl. Sci. Res.* **16**, 149–161.

Hon, T. L. & Walker, J. D. A. 1991 Evolution of hairpin vortices in a shear flow. *Computers Fluids* **20**, 343–358.

Hultgren, L. S. & Gustavsson, L. H. 1981 Algebraic growth of disturbances in a laminar boundary layer. *Phys. Fluids* **24**, 1000–1004.

Kendall, J. M. 1985 Experimental study of disturbances produced in a pretransitional laminar boundary layer by weak free-stream turbulence. *AIAA Paper* 85-1695.

Kendall, J. M. 1990 Boundary layer receptivity to freestream turbulence. *AIAA Paper* 90-1504.

Klebanoff, P. S. 1971 Effect of free-stream turbulence on a laminar boundary layer. *Bull. Am. Phys. Soc.* **16**, 1323.

Klebanoff, P. S., Tidstrom, K. D. & Sargent, L. M. 1962 The three-dimensional nature of boundary layer instability. *J. Fluid Mech.* **12**, 1–34.

Kyriakides, N. K., Kastrinakis, E. G., Nychas, S. G. & Goulas, A. 1999 Aspects of flow structure during a cylinder wake-induced laminar/turbulent transition. *AIAA J.* **37**, 1197–1205.

Landahl, M. T. 1980 A note on an algebraic instability of inviscid parallel shear flows. *J. Fluid Mech* **98**, 243–251.

Leib, S. J., Wundrow, D. W. & Goldstein, M. E. 1999 Effect of free-stream turbulence and other vortical disturbances on a laminar boundary layer. *J. Fluid Mech* **380**, 169–203.

Lu, L. J. & Smith, C. R. 1985 Image processing of hydrogen bubble flow visualization for determination of turbulence statistics and bursting characteristics. *Exps. Fuids* **3**, 349–356.

Luchini, P. 2000 Reynolds-number-independent instability of the boundary layer over a flat surface: optimal perturbations. *J. Fluid Mech* **404**, 289–309.

Matsubara, M. & Alfredsson, P. H. 2001 Disturbance growth in boundary layers subjected to free-stream turbulence. *J. Fluid Mech.* **430**, 149–168.

Mayle, R. E. 1991 The role of laminar-turbulent transition in gas turbine engines. *Trans. ASME: J. Turbomach.* **113**, 509–537.

Meinhart, C. D. & Adrian, R. J. 1995 On the existence of uniform momentum zones in a turbulent boundary layer. *Phys. Fluids* **7**, 694–696.

Mislevy, S. P. & Wang, T. 1996 The effects of adverse pressure gradients on momentum and thermal structures in transitional boundary layers: Part i- mean quantities. *Trans. ASME: J Turbomach.* **118**, 717–727.

Morkovin, M. V. 1969 On the many faces of transition. In *Viscous Drag Reduction* (ed. G. S. Wells), pp. 1–31. Plenum.

Nagarajan, S., Lele, S. K. & Ferziger, J. H. 2007 Leading-edge effects in bypass transition. *J. Fluid Mech.* **572**, 471–504.

Ovchinnikov, V., Piomelli, U. & Choudhari, M. M. 2006 Numerical simulations of boundary-layer transition induced by a cylinder wake. *J. Fluid Mech.* **547**, 413–441.

Robinson, S. K. 1991 Coherent motions in the turbulent boundary layer. *Annu. Rev. Fluid Mech.* **23**, 601–639.

Savill, A. & Zhou, M. 1983 Floquet analysis of secondary instability in shear flows. In *Proc. the 2nd Asian Congress of Fluid Mechanics* (ed. M. C. KoN), pp. 743–754. Science Press.

Schoppa, W. & Hussain, F. 2002 Coherent structure generation in near-wall turbulence. *J. Fluid Mech.* **453**, 57–108.

Shukhman, I. G. 2006 Evolution of a localized vortex in plane nonparallel viscous flows with constant velocity shear. i. hyperbolic flow. *Phys. Fluids* **18**, 097101.

Shukhman, I. G. 2007 Evolution of a localized vortex in plane nonparallel viscous flows with constant velocity shear. ii. elliptic flow. *Phys. Fluids* **19**, 017106.

Singer, B. A. & Joslin, R. D. 1994 Metamorphosis of a hairpin vortex into a young turbulent spot. *Phys. Fluids* **6**, 3724–3736.

Skote, M., Haritonidis, J. H. & Henningson, D. S. 2002 Varicose instabilities in turbulent boundary layers. *Phys. Fluids* **14**, 2309–2323.

Smith, C. R. & Walker, J. D. A. 1997 Sustaining mechanisms of turbulent boundary layers: The role of vortex development and interactions. In *Self-Sustaining Mechanisms of Wall Turbulence* (ed. R. L. Panton). Advances in Fluid Mechanics, vol. 15, pp. 13–47. Computational Mechanics Publications.

Squire, L. C. 1989 Interactions between wakes and boundary layers. *Prog. Aerospace Sci.* **26**, 261–288.

Suponitsky, V., Cohen, J. & Bar-Yoseph, P. Z. 2005 The generation of streaks and hairpin vortices from a localized vortex disturbance embedded in unbounded uniform shear flow. *J. Fluid Mech.* **535**, 65–100.

Svizher, A. & Cohen, J. 2006 Holographic particle image velocimetry measurements of hairpin vortices in a subcritical air channel flow. *Phys. Fluids* **18**, 014105.

Tumin, A. & Reshotko, E. 2001 Spatial theory of optimal disturbances in boundary layers. *Phys. Fluids* **13**, 2097–2104.

Westin, K. J. A., Bakchinov, A. A., Kozlov, V. V. & Alfredsson, P. H. 1998 Experiments on localized disturbances in a flat boundary layer. part i: The receptivity and evolution of a localized free stream turbulence. *Eur. J. Mech.* B/*Fluids* **17**, 823–846.

Willert, C. E. & Gharib, M. 1991 Digital particle image velocimetr. *Exps. Fluids* **10**, 181–193.

Zhou, J., Adrian, R. J., Balachandar, S. & Kendall, T. M. 1999 Mechanism for generating coherent packets of hairpin vortices in channel flow. *J. Fluid Mech.* **387**, 353–396.

Zhou, M. D. & Squire, L. C. 1985 the interaction of a wake with a turbulent boundary-layer. *J. Aeronaut.* **89**, 72–81.